JACS
JOURNAL OF THE AMERICAN CHEMICAL SOCIETY

Subscriber access provided by ISTANBUL TEKNIK UNIV

Article

A Quasi-Time-Resolved CryoTEM Study of the Nucleation of CaCO under Langmuir Monolayers

Benot P. Pichon, Paul H. H. Bomans, Peter M. Frederik, and Nico A. J. M. Sommerdijk

J. Am. Chem. Soc., **2008**, 130 (12), 4034-4040 • DOI: 10.1021/ja710416h

Downloaded from http://pubs.acs.org on February 8, 2009

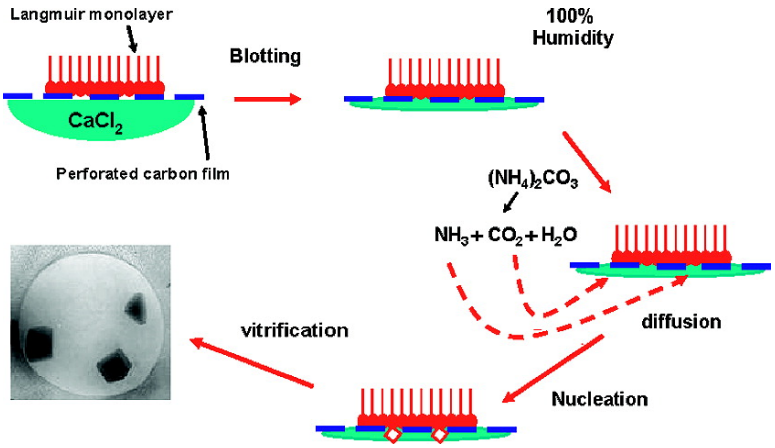

More About This Article

Additional resources and features associated with this article are available within the HTML version:

- Supporting Information
- Links to the 1 articles that cite this article, as of the time of this article download
- Access to high resolution figures
- Links to articles and content related to this article
- Copyright permission to reproduce figures and/or text from this article

View the Full Text HTML

ACS Publications
High quality. High impact.

Journal of the American Chemical Society is published by the American Chemical Society. 1155 Sixteenth Street N.W., Washington, DC 20036

J|A|C|S
ARTICLES
Published on Web 02/28/2008

A Quasi-Time-Resolved CryoTEM Study of the Nucleation of $CaCO_3$ under Langmuir Monolayers

Benoît P. Pichon,[†] Paul H. H. Bomans,[‡,§] Peter M. Frederik,[‡,§] and Nico A. J. M. Sommerdijk*[,†,‡]

Laboratory for Macromolecular and Organic Chemistry and Soft Matter CryoTEM Research Unit, Biomedical Engineering Department, Eindhoven University of Technology, P.O. Box 513, 5600 MB Eindhoven, The Netherlands, and Department of Pathology, Electron Microscopy Unit, University of Maastricht, The Netherlands

Received November 18, 2007; E-mail: N.Sommerdijk@tue.nl

Abstract: Calcium carbonate biomineralization uses complex assemblies of macromolecules that control the nucleation, growth, and positioning of the mineral with great detail. To investigate the mechanisms involved in these processes, for many years Langmuir monolayers have been used as model systems. Here, we descibe the use of cryogenic transmission electron microscopy in combination with selected area electron diffraction as a quasi-time-resolved technique to study the very early stages of this process. In this way, we assess the evolution of morphology, polymorphic type, and crystallographic orientation of the calcium carbonate formed. For this, we used a self-assembled Langmuir monolayer of a valine-based bisureido surfactant (**1**) spread on a $CaCl_2$-containing subphase and deposited on a holey carbon TEM grid. In a controlled environment, the grid is exposed to an atmosphere containing NH_3 and CO_2 (the $(NH_4)_2CO_3$ diffusion method) for precisely determined periods of time (reaction times 30−1800 s) before it was plunged into melting ethane. This procedure allows us to observe amorphous calcium carbonate (ACC) particles growing from a few tens of nanometers to hundreds of nanometers and then crystallizing to form [00.1] oriented vaterite. The vaterite in turn transforms to yield [10.0] oriented calcite. We also performed the reaction in the absence of monolayer or in the presence of a nondirective monolayer of surfactant containing an oligo(ethylene oxide) **2** head group. Both experiments also showed the formation of a transient amorphous phase followed by a direct conversion into randomly oriented calcite crystals. These results imply the specific though temporary stabilization of the (00.1) vaterite by the monolayer. However, experiments performed at higher $CaCl_2$ concentrations show the direct conversion of ACC into [10.0] oriented calcite. Moreover, prolonged exposure to the electron beam shows that this transformation can take place as a topotactic process. The formation of the (100) calcite as final product under different conditions shows that the surfactant is very effective in directing the formation of this crystal plane. In addition, we present evidence that more than one type of ACC is involved in the processes described.

Introduction

Many organisms use calcium carbonate mineralization to form precisely shaped and composed materials specifically designed for a variety of functions, including support and defense. To this end, they use complex assemblies of macromolecules that control the nucleation, growth, and positioning of the mineral with great detail.[1] Although many details of this process are not yet understood, it has been demonstrated that nucleation and growth are often controlled by acidic macromolecules such as polypeptides rich in aspartate and glutamate residues and sulfonated polysaccharides.[2] Polypeptides with organized domains present within a macromolecular matrix have been associated with the nucleation of calcium carbonate biominerals.[3] To elucidate the mechanisms involved, researchers have used different synthetic systems to study the controlled formation of oriented $CaCO_3$ crystals in vitro.[4] In particular, organic 2D assemblies such as substrate adsorbed polymers,[5,6] Langmuir,[7−10] Langmuir−Blodgett,[11,12] and self-assembled[13−16] monolayers have been instrumental in the study of the nucleation and growth of such crystals.

In many studies, the structure of the stabilized crystal face was compared with the available information on the monolayer

[†] Laboratory for Macromolecular and Organic Chemistry, Eindhoven University of Technology.

[‡] Soft Matter CryoTEM Research Unit, Eindhoven University of Technology.

[§] University of Maastricht.

(1) (a) Addadi, L.; Weiner, S. *Angew. Chem., Int. Ed.* **1992**, *31*, 153−169. (b) Meldrum, F. C. *Int. Mater. Rev.* **2003**, 187−224. (c) Mann, S. *Biomineralization: Principles and Concepts in Bioinorganic Materials Chemistry;* Oxford University Press: New York, 2001.

(2) Nudelman, F.; Chen, H. H.; Goldberg, H. A.; Weiner, S.; Addadi, L. *Faraday Discuss.* **2007**, *136*, 9−25.

(3) Addadi, L.; Weiner, S. *Proc. Natl. Acad. Sci. U.S.A.* **1985**, *82*, 4110−4114.

(4) (a) Lam, R. S. K.; Charnock, J. M.; Lennie, A.; Meldrum, F. C. *CrystEngComm* **2007**, *9*, 1226−1236. (b) Pokroy, B.; Zolotoyabko, E.; Amir, N. *Biomacromolecules* **2006**, *7*, 550−556.

(5) Addadi, L.; Moradian, J.; Shay, E.; Maroudas, N. G.; Weiner, S. *Proc. Natl. Acad. Sci. U.S.A.* **1987**, *84*, 2732−2736.

(6) Donners, J. J. J. M.; Nolte, R. J. M.; Sommerdijk, N. A. J. M. *J. Am. Chem. Soc.* **2002**, *124*, 9700−9701.

 10.1021/ja710416h CCC: $40.75 **© 2008 American Chemical Society**

organization. From this comparison, the authors extracted information concerning the relationship between the template and the developing mineral phase. This has led to the nomination of different important factors involved in the nucleation process, including epitaxial,[17] stereochemical[3] and orientational matching,[6,11,12] electrostatic interactions,[10] and template adaptability.[4] In most cases, the information concerning the crystallographic orientation and morphology of the crystals was obtained by isolation of crystals large enough to be analyzed with the available methods.

The nucleation face of a crystal can be determined, establishing its orientation with respect to the template in several ways. These include measuring the angles between the exposed known crystal planes,[10,12,14] modeling the crystal shape,[8a,b] or determining the relative intensities of the X-ray reflections.[14,18] These methods, however, can only be applied generally for crystals that have sizes near or in the micrometer range and do not give information about the orientation of the mineral in the very early stages of the experiment (i.e., on the onset of nucleation). Moreover, several examples are known in which crystals are suspected to change their orientation with respect to the air−water interface in the course of their development.[5a,b] A frequently used method to obtain information on the early stages of crystal growth involves the transfer of these crystals to a transmission electron microscopy (TEM) grid and the subsequent analysis by selected area electron diffraction (SAED). As gravity will cause these crystals to lie on their largest exposed plane, not necessarily on their nucleation plane, it is difficult to fulfill the strict requirement that the orientation of the nucleation plane with respect to electron beam is unambiguously known. Moreover, forced precipitation from supersaturated solution caused by the drying of the sample can cause artifacts and leave some ambiguity about when and where nucleation did take place.[19]

Although in situ experiments such as X-ray microscopy[20] and synchrotron small-angle X-ray scattering[21] have revealed important information on the formation of $CaCO_3$ in solution, little information is available on the interaction of the organic and inorganic phases during the process. Using in situ infrared and in situ UV experiments, other researchers have demonstrated the adaptation of the monolayer during the process.[11,12] In addition, in situ grazing incidence X-ray diffraction and reflectivity experiments indicated an absence of structural matching between the two phases.[22] Moreover, important indications have been found for the involvement of amorphous calcium carbonate (ACC) as a transient precursor phase in the formation of $CaCO_3$.[23] Nevertheless, to date, it has not been possible to unambiguously establish how the template drives the nucleation of specific crystal faces.[24]

In recent years, the use of cryogenic transmission electron microscopy (cryoTEM) has been applied to study molecular assemblies,[25] including monolayers,[26,27] in vitrified specimens. CryoTEM has already been applied to study the formation of silica-based organic/inorganic hybrid materials.[28] Here, we present a cryoTEM-based method that allows us to assess the morphology, polymorphic type, and orientation of calcium carbonate in the very early stages of formation. In this new setup, we use plunge freezing of the sample to arrest the growth process and cryoTEM in combination with SAED to analyze the resulting crystals in their native hydrated state and in their original orientation. As a template, we use a valine-based bisurea

(7) (a) Mann, S.; Heywood, B. R.; Rajam, S.; Birchall, J. D. *Nature* **1988**, *334*, 692−695. (b) Mann, S.; Heywood, B. R.; Rajam, S.; Walker, J. B. A.; Davey, R. J.; Birchall, J. D. *Adv. Mater.* **1990**, *2*, 257−261. (c) Rajam, S.; Heywood, B. R.; Walker, J. B. A.; Mann, S.; Davey, R. J.; Birchall, J. D. *J. Chem. Soc., Faraday Trans.* **1991**, *87*, 727−734. (d) Heywood, B. R.; Mann, S. *Chem. Mater.* **1994**, *6*, 311−318. (e) Didymus, J. M.; Mann, S.; Benton, W. J.; Collins, I. R. *Langmuir* **1995**, *11*, 3130−3136. (f) Champ, S.; Dickinson, J. A.; Fallon, P. S.; Heywood, B. R.; Mascal, M. *Angew. Chem., Int. Ed.* **2000**, *39*, 2716−2719. (g) Buijnsters, P. J. J. A.; Donners, J. J. J. M.; Hill, S. J.; Heywood, B. R.; Nolte, R. J. M.; Zwanenburg, B.; Sommerdijk, N. A. J. M. *Langmuir* **2001**, *17*, 3623−3628. (h) DiMasi, E.; Patel, V. M.; Sivakumar, M.; Olszta, M. J.; Yang, Y. P.; Gower, L. B. *Langmuir* **2002**, *18*, 8902−8909.

(8) (a) Cavalli, S.; Popescu, D. C.; Tellers, E. E.; Vos, M. R. J.; Pichon, B. P.; Overhand, M.; Rapaport, H.; Sommerdijk, N. A. J. M.; Kros, A. *Angew. Chem., Int. Ed.* **2006**, *45*, 739−744. (b) Popescu, D. C.; Smulders, M. M. J.; Pichon, B. P.; Chebotareva, N.; Kwak, S.-Y.; van Asselen, O. L. J.; Sijbesma, R. P.; DiMasi, E.; Sommerdijk, N. A. J. M. *J. Am. Chem. Soc.* **2007**, *129*, 14058−14067. (c) Pichon, B. P.; Cantin, S.; Smulders, M. M. J.; Vos, M. R. J.; Cheborateroya, N.; Popescu, D. C.; van Asselen, O.; Perrot, F.; Sijbesma, R.; Sommerdijk, N. A. J. M. *Langmuir* **2007**, *23*, 12655−16662.

(9) DiMasi, E.; Kwak, S.-Y.; Pichon, B. P.; Sommerdijk, N. A. J. M. *CrystEngComm* **2007**, *9*, 1192−1204.

(10) (a) Volkmer, D.; Fricke, M.; Agena, C.; Mattay, J. *CrystEngComm* **2002**, *4*, 288−295. (b) Volkmer, D.; Fricke, M.; Huber, T.; Sewald, N. *Chem. Commun.* **2004**, *16*, 1872−1873. (c) Volkmer, D.; Fricke, M.; Agena, C.; Mattay, J. *J. Mater. Chem.* **2004**, *14*, 2249−2259.

(11) Ahn, D. J.; Berman, A.; Charych, D. *J. Phys. Chem.* **1996**, *100*, 12455−12461.

(12) Berman, A.; Ahn, D. J.; Lio, A.; Salmeron, M.; Reichert, A.; Charych, D. *Science* **1995**, *269*, 515−518.

(13) Archibald, D. D.; Quadri, S. B.; Gaber, B. P. *Langmuir* **1996**, *12*, 538−546.

(14) Aizenberg, J.; Black, A. J.; Whitesides, G. M. *J. Am. Chem. Soc.* **1999**, *121*, 4500−4509.

(15) Travaille, A. M.; Donners, J. J. J. M.; Gerritsen, J. W.; Sommerdijk, N. A. J. M.; Nolte, R. J. M.; van Kempen, H. *Adv. Mater.* **2002**, *14*, 492−495.

(16) (a) Wurm, D. B.; Brittain, S. T.; Kim, Y.-T. *J. Mater. Sci. Lett.* **1996**, *15*, 1285−1287. (b) Küther, J.; Nelles, G.; Seshadri, R.; Schaub, M.; Butt, H.-J.; Tremel, W. *Chem.−Eur. J.* **1998**, *4*, 1834−1842. (c) Küther, J.; Seshadri, R.; Tremel, W. *Angew. Chem., Int. Ed.* **1998**, *37*, 3044−3047. (d) Aizenberg, J.; Black, A. J.; Whitesides, G. M. *Nature* **1998**, *394*, 868−871. (e) Aizenberg, J.; Black, A. J.; Whitesides, G. M. *Nature* **1999**, *398*, 495−498.

(17) Lahiri, J.; Xu, G.; Dabbs, D. M.; Yao, N.; Aksay, I. A.; Groves, J. T. *J. Am. Chem. Soc.* **1997**, *119*, 5449−5450.

(18) Sommerdijk, N. A. J. M.; van Leeuwen, E. N. M.; Vos, M. R. J.; Jansen, J. A. *CrystEngComm* **2007**, *9*, 1209−1214.

(19) This point is raised in Tracy, S. L.; Williams, D. A.; Jennings, H. M. *J. Cryst. Growth* **1998**, *193*, 382−388.

(20) Rieger, J.; Thieme, J.; Schmidt, C. *Langmuir* **2000**, *16*, 8300−8305.

(21) Bolze, J.; Peng, B.; Dingenouts, N.; Panine, P.; Narayanan, T.; Ballauff, M. *Langmuir* **2002**, *18*, 8364−8369.

(22) DiMasi, E.; Olszta, M. J.; Patel, V. M.; Gower, L. B. *CrystEngComm* **2003**, *5*, 346−350.

(23) (a) Brecevic, A. L.; Nielsen, A. A. *J. Cryst. Growth* **1989**, *98*, 504−510. (b) Aizenberg, J.; Lambert, G.; Addadi, L.; Weiner, S. *Adv. Mater.* **1996**, *8*, 222−226. (c) Beniash, E.; Aizenberg, J.; Addadi, L.; Weiner, S. *Proc. R. Soc. London, Ser. B* **1997**, *264*, 461−465. (d) Beniash, E.; Addadi, L.; Weiner, S. *J. Struct. Biol.* **1999**, *125*, 50−62. (e) Politi, Y.; Mahamid, J.; Goldberg, H.; Weiner, S.; Addadi, L. *CrystEngComm* **2007**, *9*, 1171−1177.

(24) (a) Lee, J. R. I.; Han, Y.-J.; Willey, T. M.; Wang, D.; Meulenberg, R. W.; Nilsson, J.; Dove, P. M.; Terminello, L. J.; van Buuren, T.; De Yoreo, J. J. *J. Am. Chem. Soc.* **2007**, *129*, 10370−10381. (b) Han, T. Y.-J.; Aizenberg, J. *Chem. Mater.* **2008**, *20*, 1064−1068.

(25) (a) Frederik, P. M.; Sommerdijk, N. A. J. M. *Curr. Opin. Colloid Interface Sci.* **2005**, *10*, 245−249. (b) Goldraich, M.; Talmon, Y. *Amphiphilic Block Copolym.* **2000**, 253−280.

(26) (a) Majewski, J.; Margulis, L.; Jacquemain, D.; Leveiller, F.; Bohm, C.; Arad, T.; Talmon, Y.; Lahav, M.; Leiserowitz, L. *Science* **1993**, *261*, 899−902.

(27) Vos, M. R. J.; Bomans, P. H. H.; de Haas, F.; Frederik, P. M.; Jansen, J. A.; Nolte, R. J. M.; Sommerdijk, N. A. J. M. *J. Am. Chem. Soc.* **2007**, *129*, 11894−118945.

(28) (a) Regev, O. *Langmuir* **1996**, *12*, 4940−4944. (b) Sun, Q.; Kooyman, P. J.; Grossmann, J. G.; Bomans, P. H. H.; Frederik, P. M.; Magusin, P. C. M. M.; Beelen, Th. P. M.; van Santen, R. A.; Sommerdijk, N. A. J. M. *Adv. Mater.* **2003**, *15*, 1097−1100. (c) Pevzner, S.; Regev, O.; Lind, A.; Lindén, M. *J. Am. Chem. Soc.* **2003**, *125*, 652−653.

(29) For other examples of self-organized bisurea surfactant systems, see also: (a) Chebotareva, N.; Bomans, P. H. H.; Frederik, P. M.; Sommerdijk, N. A. J. M.; Sijbesma, R. P. *Chem. Commun.* **2005**, 4967−4969. (b) Vos, M. R. J.; Etxebarria, J. G.; Llanes Pallas, A.; Breurken, M.; van Asselen, O. L. J.; Bomans, P. H. H.; Frederik, P. M.; Nolte, R. J. M.; Sommerdijk, N. A. J. M. *J. Am. Chem. Soc.* **2005**, *127*, 16768−16769. (c) Moreau, J. J. E.; Pichon, B. P.; Bied, C.; Man, M. W. C. *J. Mater. Chem.* **2005**, *15*, 3929−3936.

Chart 1. Chemical Structures of the Valine-Based (**1**)[8b] and the Penta(ethylene oxide)-Derived (**2**)[8c] Bisurea Surfactants

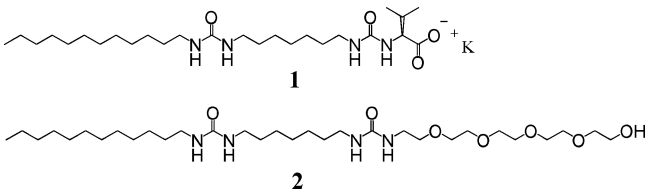

amphiphile **1**,[8b,15] which self-organizes by strong bifurcated hydrogen bonding between the urea units (Chart 1).[29]

Results

Experimental Design. In the experimental setup used (Figure 1), Langmuir monolayers were prepared in glass crystallization dishes containing a subphase of aqueous 10 mM $CaCl_2$. The crystallization dish was placed inside a glovebox[27] fitted to a vitrification robot (step 1), which allowed us to maintain the sample at a controlled temperature (22 °C) and at 100% relative humidity. Before the experiment, the equipment was flushed with nitrogen gas to prevent it from reacting with the CO_2 from the air, which would create an off-set in the time-dependent $CaCO_3$ formation (Supporting Information S2). Subsequently, the monolayer was deposited onto a holey carbon-coated TEM grid by slowly draining the aqueous solution through a valve on the bottom of the glass dish (step 2). In this way, the monolayer became suspended over the 2-μm holes in the carbon film covering the grid while still in contact with the $CaCl_2$ solution. Maintaining the same environmental conditions, we then transferred the grids into the chamber of the fully automated vitrification robot (step 3). In there, the excess liquid was removed by automated blotting to produce an approximately 100-nm thin aqueous layer under the monolayer (step 4). After this ($t = 0$), a 10 mM aqueous ammonium carbonate solution was sprayed in the chamber using the Vitrobot humidification system. Because of the decomposition of ammonium carbonate $(NH_4)_2CO_3$, the atmosphere inside the chamber became saturated with ammonia (NH_3) and carbon dioxide (CO_2) (step 5). The diffusion of these components into the aqueous film led to the concomitant formation of $CaCO_3$ while maintaining 100% humidity (step 6). The reaction was allowed to proceed for precisely determined periods of time ranging from 0 to 1800 s (step 7) before the reaction was quenched by plunging the grid into melting ethane (step 8). This procedure not only provides a method to investigate the early stages of the mineralization process under the monolayer but also should trap the amorphous phase when present without staining or drying the sample. After being transferred to a cryoholder, both the morphology and the (crystallographic) orientation of the particles formed in solution can be studied using cryoTEM without disturbing them.

$CaCO_3$ Formation under a Langmuir Monolayer of Valine-Based Surfactant 1. Amorphous Calcium Carbonate Formation. Using the experimental procedure described in the Supporting Information (S2), we allowed calcium carbonate to form under a monolayer of the valine-based bisurea surfactant **1**, which had been spread on an aqueous subphase containing 10 mM $CaCl_2$ (Figure S3). The reaction was terminated by plunging the system into melting ethane after different periods

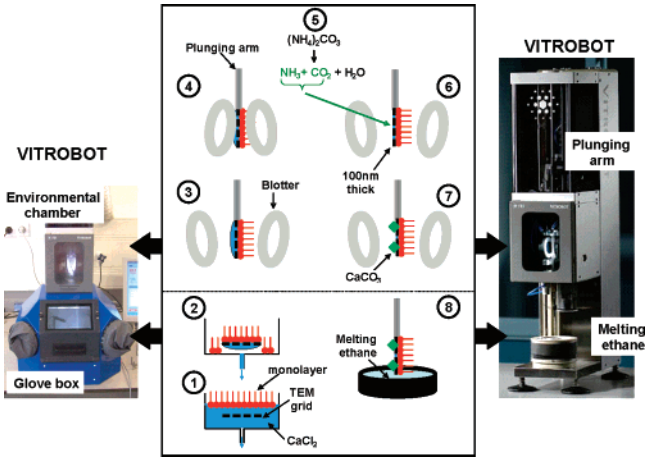

Figure 1. Schematic representation of the setup for the preparation of cryoTEM samples from the mineralization process. (1) Deposition of the monolayer on a $CaCl_2$ solution. (2) Draining of the solution to deposit the monolayer on the TEM grid. (3) Grid mounted on the plunging arm and introduction in the environmental chamber of the vitrobot. (4) Blotting of the sample to remove the excess $CaCl_2$ solution. (5) Introduction of $(NH_4)_2CO_3$ and its decomposition into NH_3 and CO_2. (6) Diffusion of NH_3 and CO_2 into the solution. (7) Formation of $CaCO_3$. (8) Quenching of the reaction.

of time ranging from 30 s to 30 min. During the very early stages (30 s to 2 min), we observed the formation of small spherical particles that increased in size as well as in number during this period (Figure 2). More precisely, after 30 s the particles had sizes between 10 and 50 nm (average 35 nm) and displayed a density of 50 particles/μm^2. After 1 min, the particle density was similar while their sizes had increased slightly to 20−70 nm (average 50 nm). After 2 min, the size range covered 50−120 nm (average 100 nm) with a particle density of 100 μm^{-2}. Significantly, the clustering of particles was now also observed.

The observed particles were absent in control experiments in which no ammonium carbonate was introduced in the system (Figure S2). This demonstrates not only that in the experimental setup used the reaction with CO_2 from the air does not play a significant role, but also that the particles can be differentiated from contaminating ice particles frequently observed in cryo-TEM preparations.[30] SAED showed the absence of diffraction spots in all samples prepared in the presence of $NH_4(CO_3)_2$ during these early stages, suggesting that the particles consisted of ACC. During the cryoTEM experiments, it became apparent that the ACC particles could be divided into two classes. Whereas the larger particles (>30 nm) were persistent in the electron beam upon application of higher electron doses (3000 e Å^2), the smaller particles with diameters of 20−30 nm disintegrated under the same conditions (Figure 3, arrows) Interestingly, earlier reports similarly have suggested the existence of multiple forms of ACC not only with a different degree of hydration, but also with a different degree of short range order.[31] We speculate that our results may be related to these observations.

Formation of Vaterite. When the reaction time was increased to 3 min, two types of particles were observed: a population of small particles coexisting with a few distinctly larger ones (Figure 2d). The smaller category was present with a particle

(30) Dubochet, J.; Adrian, M.; Chang, J.-J.; Homo, J.-C.; Lépault, J.; McDowall, A. W.; Schultz, P. *Q. Rev. Biophys.* **1988**, *21*, 129−288.

(31) Politi, Y.; Levi-Kalisman, Y.; Raz, S.; Wilt, F.; Addadi, L.; Weiner, S.; Sagi, I. *Adv. Funct. Mater.* **2006**, *16*, 1289−1298.

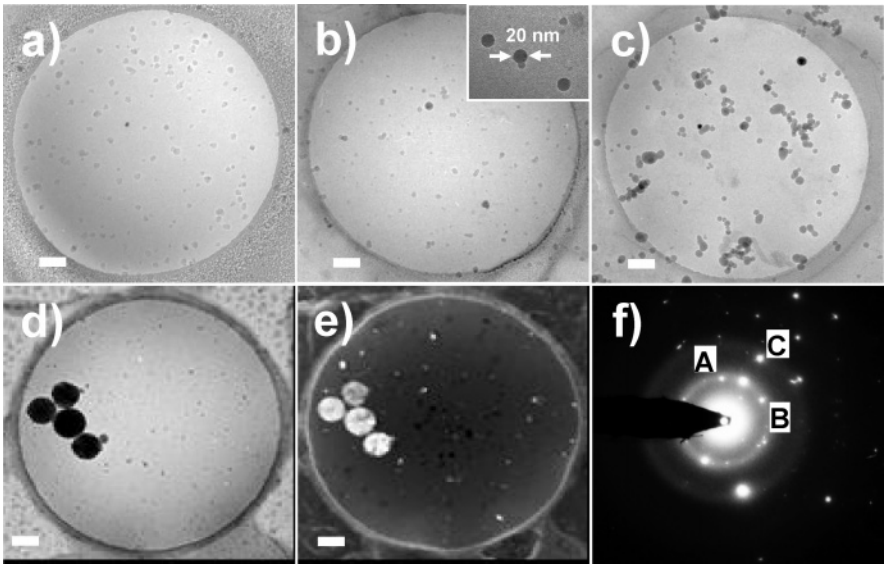

Figure 2. TEM pictures of particles grown from a monolayer of valine-based surfactant **1** in the holes of the TEM grid after reaction times of (a) 30 s, (b) 1 min, (c) 2 min, and (d) 3 min. Scale bars are 200 nm. (e, f) Dark field TEM pictures and SAED pattern of the whole hole shown in (d), respectively. The dark field picture corresponds to spot "C". Reflections for (f): $A = (100)$, $d = 3.58$ Å; $B = (110)$, $d = 3.58$ Å; $C = (010)$, $d = 3.58$ Å; $(A \wedge B) = 30°$; $(A \wedge C) = 60°$; zone axis [00.1] of vaterite. The appearance of white spots in the dark field image (Figure 1e) that do not correlate to particles in the corresponding bright field image (Figure 1d) is attributed to beam-induced ice crystallization (see also Figure S3).

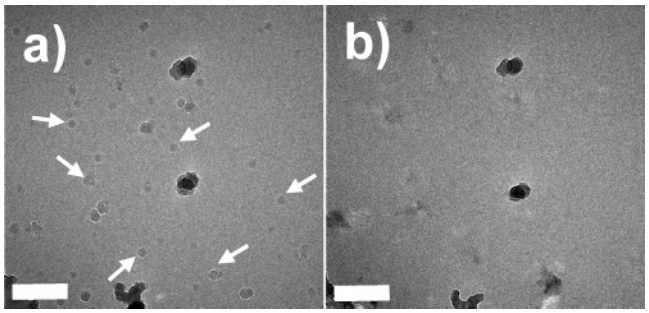

Figure 3. TEM images of particles grown after 2 min of reaction and exposed under a beam that corresponds to an electron density of (a) 100 e Å^2 and (b) 3000 e Å^2. Arrows in (a) show some of the particles that disappear in (b).

density of $\sim 30\ \mu m^{-2}$ and had diameters < 30 nm, hence, clearly smaller than those observed after 2 min. In contrast, the few larger particles had sizes exceeding 200 nm. The absence of diffraction spots in SAED for the smaller ones suggests that these still consisted of ACC. In contrast, the larger ones all diffracted as [00.1] oriented vaterite (Figure 2f). The observation of exclusively [00.1] oriented vaterite may be related to a directing effect of the surfactant molecules in the monolayer, similar to what has been reported for fully compressed monolayers of stearic acid.[7a]

Our observation that the dimensions of the ACC particles present after 3 min were smaller than those observed in the earlier stages of calcium carbonate formation (between 30 s and 2 min) suggests that the larger particles grow at the expense of the smaller ones through Ostwald ripening, a dissolution/reprecipitation mechanism driven by the reduction of total surface free energy. Importantly, dark field images (Figure 2e) revealed that these particles, although they presented a single diffraction pattern, had not yet fully crystallized and were still partially composed of amorphous material. The presence of small (<20 nm) particles decorating the surface of the larger crystalline ones may indicate that the latter ones further grow through addition of the former ones. However, at this point we cannot exclude that these satellite particles may be the seed of new crystals that are growing in the proximity of the other clustered ones.

Calcite Formation. When the calcium carbonate formation under monolayers of **1** was allowed to proceed for 5 min, the cryoTEM images became dominated by larger particles (particle density 6 μm^{-2}) with sizes > 100 nm (Figure 4a,c). However, a population of particles with sizes of 0−50 nm was also still present (particle density 3 μm^{-2}). SAED demonstrated that approximately 65% of the larger particles diffracted as (00.1) vaterite (Figure 4b), whereas the remaining 35% consisted of calcite, almost exclusively in a [10.0] orientation (Figure 4e). It was not possible to unambiguously determine the crystallinity of the smaller particles as in almost all cases the selected area also overlapped with the larger crystalline ones.

After 10 min, the number of crystals had increased over all size ranges (Figure 4d,f). The crystal density now amounted to 28 μm^{-2} with approximately half of these <100 nm (14 particles/μm^2). Of this population, approximately 70% consisted of (10.0) calcite, indicating that in this stage of the process (5−10 min after the start of the reaction) calcite crystals are continuously nucleating. It also suggests that the smaller crystals of calcite found after 5 min may be freshly nucleated calcite crystals.

Importantly, the same preferred [10.0] orientation of calcite was found, similar to that for the experiments performed using the Kitano protocol, which involves the crystallization of $CaCO_3$ from a supersaturated calcium bicarbonate solution controlled by CO_2 outgassing.[32] This demonstrates that the monolayer of **1** is able to stabilize the same specific crystal face of calcite regardless of the kinetic details associated with the different procedures.[5b] It is interesting to note that all particles have a spherical appearance (as judged by their 2D projections) when their dimensions are <100 nm. Although vaterite has a hexagonal lattice, the observed larger crystals generally appear

(32) Kitano, Y.; Park, K.; Hood, D. W. *J. Geophys. Res.* **1963**, *67*, 4873−4874.

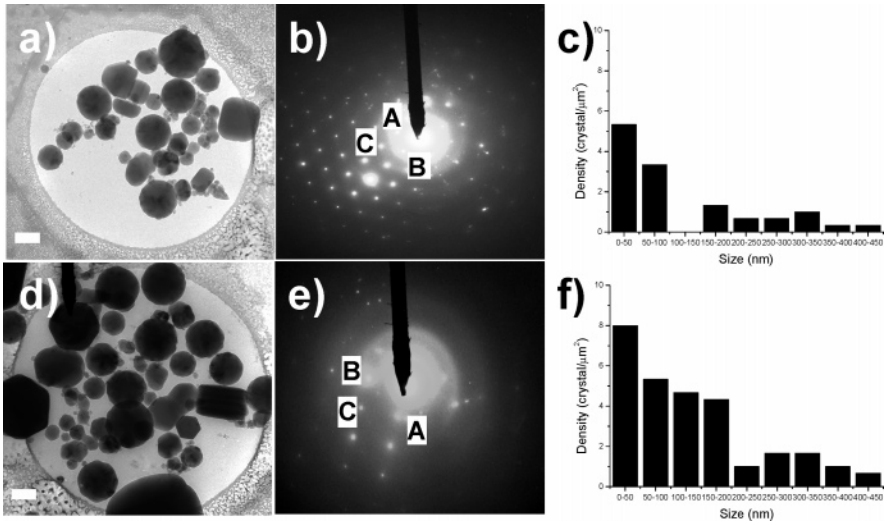

Figure 4. $CaCO_3$ formed after (a−c) 5 min and (d−f) 10 min of reaction. (a, d) TEM pictures, (b, e) SAED patterns, and (c, f) particles size distributions. Scale bars are 200 nm. Reflections for (b): $A = (100)$, $d = 3.58$ Å; $B = (010)$, $d = 3.58$ Å; $C = (110)$, $d = 3.58$ Å; $(A \wedge B) = 60°$; $(A \wedge C) = 30°$; zone axis [00.1] of vaterite. Reflections for (e): $A = (006)$, $d = 2.84$ Å; $B = (110)$, $d = 2.495$ Å; $C = (116)$, $d = 1.87$ Å; $(A \wedge B) = 90°$; $(A \wedge C) = 45°$; zone axis [10.0] of calcite.

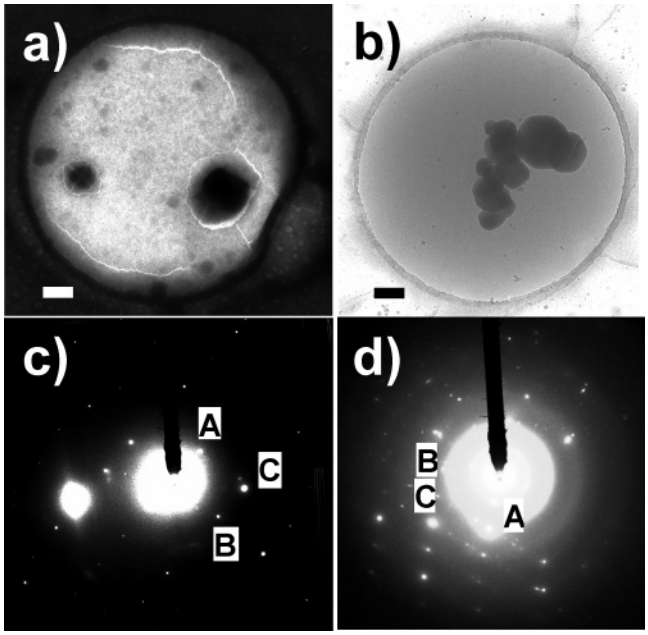

Figure 5. TEM pictures showing particles grown in the presence of a 100 mM $CaCl_2$ solution after (a) 5 min and (b) 30 min. Scale bars are 200 nm. (c, d) Corresponding SAED patterns. Reflections for (c): $A = (006)$, $d = 2.84$ Å; $B = (110)$, $d = 2.495$ Å; $C = (116)$, $d = 1.87$ Å; $(A \wedge B) = 90°$; $(A \wedge C) = 45°$; zone axis [10.0] of calcite. Reflections for (d): $A = (0-21)$, $d = 3.86$ Å; $B = (0\text{-}1\text{-}6)$, $d = 2.38$ Å; $C = (1\text{-}2\text{-}4)$, $d = 1.93$ Å; $(A \wedge B) = 84°$; $(A \wedge C) = 54°$; zone axis [10.0] of calcite.

as round objects, whereas the calcite crystals, because of their [10.0] orientation, appear as hexagons consistent with morphological models of [10.0] oriented calcite (Figure S5).

With reaction times exceeding 10 min, the formation of a thick layer of crystals hampered their characterization by TEM and SAED. To increase the rate of the reaction while maintaining a low nucleation density, the mineralization process was performed using a higher (100 mM) concentration of $CaCl_2$ (Figure 5). Following this procedure, after 5 min large amorphous particles with sizes of 70−200 nm were formed, whereas after 30 min only [10.0] oriented calcite was observed (Figure S4). This confirms (10.0) calcite to be the final product of the template-directed mineralization process as was indicated earlier. Significantly, exposure of the amorphous particles to the electron beam for several seconds induced the appearance of spots in the diffraction mode. Again, these patterns corresponded to calcite in its [10.0] orientation, thereby confirming the initial particles to consist of ACC.

This shows that exposure to the electron beam apparently provides enough energy to allow transformation of the ACC into one of the crystalline polymorphs, even in a vitrified ice film. Furthermore, it allowed the particle to transform into a crystal with the same shape. A similar topotactic transformation of ACC into calcite was, albeit at room temperature, observed for regenerating sea urchin spicules[33] and also in synthetic molds.[34]

Importantly, during this process the presence of the monolayer manifested itself through stabilization of the (10.0) face of calcite. This demonstrates once more that an organic template is indeed able to direct the solid-state transformation of ACC to calcite.[35] It is also interesting to note that such an electron beam-induced transformation was not observed for the smaller ACC particles formed at lower Ca^{2+} concentration (10 mM). This may be explained by the fact that under a certain threshold diameter calcium carbonate particles are not stable in their crystalline form and hence must remain amorphous.[30] Alternatively, the difference in ease of transformation may be related to the existence of different types of ACC with different degrees of short range order.[31]

Role of the Monolayer. Mineralization in the Absence of a Monolayer. When the mineralization reaction was performed without a monolayer present, we found that after the first 30 s amorphous particles were present with size ranges between 15 and 60 nm (average size 30 nm; Figure S6). These values are slightly smaller than those observed in the presence of the

(33) Politi, Y.; Arad, T.; Klein, E.; Weiner, S.; Addadi, L. *Science* **2004**, *306*, 1161−1164.
(34) Loste, E.; Park, R. J.; Warren, J.; Meldrum, F. *Adv. Funct. Mater.* **2004**, *14*, 1211−1220.
(35) Aizenberg, J.; Muller, D. A.; Grazul, J. L.; Hamann, D. R. *Science* **2003**, *299*, 1205.

Table 1. Size and Density of Amorphous Particles Formed after 30 s of Reaction without or in Presence of Monolayer of Surfactants **1** or **2**

surfactant	size (nm)	particle density (μm^{-2})
–	30	70
1	45	50
2	50	40

monolayer and are in line with the observed higher nucleation density of 70 particles/μm^2 (Table 1).

After 2 min, a new type of larger particles with an approximate diameter of 200 nm had appeared alongside a population of smaller ones (Figure S6). Whereas the smaller ones only produced a diffuse halo indicating amorphous material, the larger ones all diffracted as randomly oriented calcite as may be expected in the absence of a directing template. The decreased particle density of 21 μm^{-2} indicates that the crystals are formed at the expense of the small ACC particles. In accordance with this suggestion, the amorphous particles still present were clearly smaller than the ones observed after 30 s and displayed diameters of <35 nm. Further investigations showed that after 5 min the entire population consisted of small (50−500 nm) calcite crystals with a particle density of ∼25 crystals/μm^2 (Figure 6a,b).

It is important to note that without the presence of the monolayer, the formation of calcite crystals occurs at a higher rate than when a templating monolayer is present. Nevertheless, during this process no signs of vaterite formation were observed. The increased rate of crystallization is most likely because the absence of the monolayer allows a more rapid diffusion of the CO_2 into the aqueous film.[36]

Mineralization under a Nondirecting Monolayer. To obtain more information on the role of the template, a monolayer was prepared from the nondirecting penta(ethylene oxide) analogue **2**.[5c,37] In this assay, after 30 s we observed the formation of amorphous particles (Figure 6d) with dimensions between 30 and 65 nm and with a density of ∼40 particles/μm^2 (Figure 6c), quite similar to that observed for surfactant **1**. At the same time, the results obtained after 5 min were comparable to those obtained without a monolayer after 2 min: we observed small amorphous particles (24 μm^{-2}, average diameter ∼15 nm; Figure 6e) with a tendency to aggregate, coexisting with a population of larger ones (diameters 200−300 nm) that diffracted as calcite. However, in contrast to the crystals formed under monolayers of **1**, these all had random orientations, confirming that the molecular structure of **1** is essential in the formation of [10.0] oriented calcite.

Notably, although the crystal size and crystal density of the reaction in the presence of **2** are comparable to the numbers observed for **1**, again no sign of vaterite formation was observed. In view of the specific [00.1] orientation of the vaterite crystals with respect to the air−water interface, one may assume an interaction between the monolayer and the nucleating vaterite crystals. Consequently, we speculate that the preaggregation of the calcium ions in the vicinity of the carboxylic acid groups in the monolayer of **1** affects the kinetics in favor of the formation of vaterite as an intermediate step before calcite is formed.

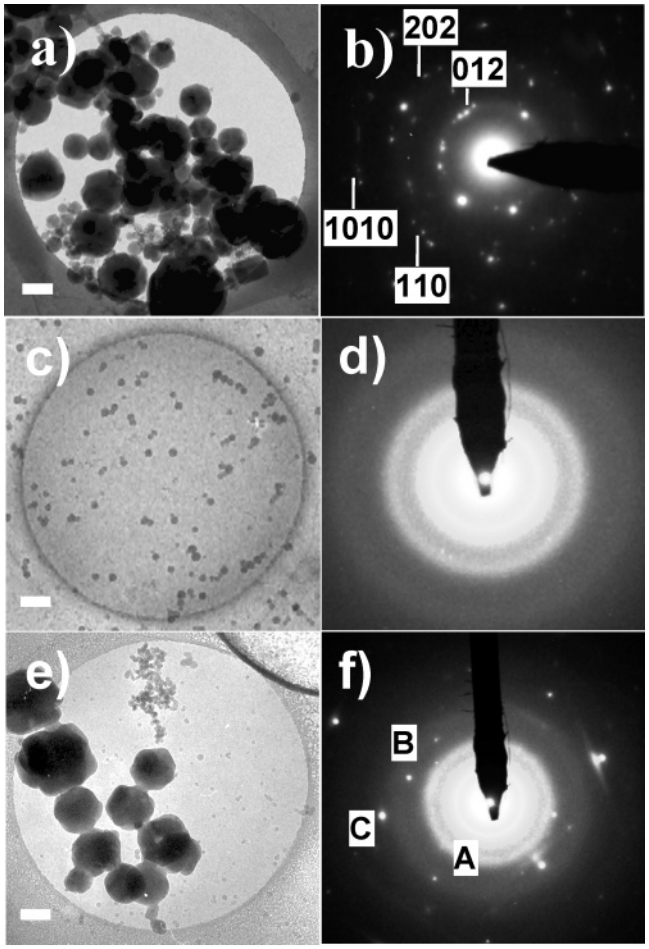

Figure 6. (a, c, e) CryoTEM pictures, scale bars are 200 nm. (b, d, f) Corresponding SAED patterns. (a, b) $CaCO_3$ crystals grown in the presence of a 10 mN $CaCl_2$ solution without any monolayer after 5 min of reaction. (c−f) Particles grown in the presence of a monolayer of **2** deposited in a 10 mN $CaCl_2$ solution. (c, d) After 30 s and (e, f) after 5 min. (d, f) Corresponding SAED patterns of (c, e). Reflections for (f): $A = 1.52$ Å (214); $B = 2.84$ Å (006); $C = 1.18$ (21 10); (A∧B) = 82°; (A∧C) = 49°; zone axis [−12.0] of calcite that is an example and corresponds to one of the crystals with a size >200 nm shown in (e).

Discussion

The monolayer of surfactant **1** directs the successive transformations from ACC to [00.1] oriented vaterite and finally to [10.0] oriented calcite. These results are in line with our previous experiments in which a monolayer of **1** was also found to lead to the stabilization of [10.0] oriented calcite.[5b] This is regardless of the fact that these previous experiments were performed following a different procedure (i.e., using the Kitano protocol).[29] Hence, the results presented here underline the effective control of the template over the nucleation of calcium carbonate.

This successive formation of the less stable phases of ACC and vaterite that precede the formation of final calcite under a monolayer of **1** is predicted by the Ostwald−Lussac law.[38] This empirical law says that first the least stable stage with the lowest density is formed, which subsequently undergoes successive

(36) Loste, E.; Díaz-Martí, E.; Zarbakhsh, A.; Meldrum, F. C. *Langmuir* **2003**, *19*, 2830−2837.
(37) Poly(ethylene oxide) chains have no significant effect on the formation of calcium carbonate. See: Colfen, H.; Qi, L. *Chem.−Eur. J.* **2001**, *7*, 106−116.
(38) (a) Ostwald, W. *Z. Phys. Chem.* **1879**, *22*, 289. (b) Söhnel, O.; Garside, J. *Precipitation;* Butterworth-Heinemann: Oxford, 1992 and references therein.

transformations until the most stable state with higher order and highest density is obtained. The kinetics in the absence of a (templating) monolayer at present give no indication for the involvement of formation vaterite, suggesting a direct conversion of ACC into calcite.

It is furthermore interesting to note that although the conversion of ACC into vaterite seems to be a solid-state transformation, the transformation of vaterite into clearly calcite proceeds through a dissolution−reprecipitation mechanism. At calcium concentrations of 10 mM, currently it is not clear whether during this transformation ACC plays a role as an intermediate, even though many calcite crystals were found to be decorated with small amorphous particles. That the direct transformation of ACC certainly is a possible route was demonstrated by the fact that at a calcium concentration of 100 mM an ACC−calcite transformation can be induced by the electron beam.

As reported in other studies, ACC with sizes in the order of tens of nanometers initially forms and aggregates into clusters.[18] ACC is formed whether or not a monolayer (charged or uncharged) is present. This shows that the formation of ACC is not affected by surface tension or supersaturation effects at the interface with the monolayer and is only induced under kinetic control. This is supported by the finding of smaller ACC particles in the presence of monolayer that act as barriers reducing the diffusion rates of CO_2 and NH_3 at the air−water interface.

The ACC particles grow through Ostwald ripening, producing a population of larger particles that subsequently crystallize to form single crystals of vaterite with spherulitic morphology as described in earlier studies.[3,39] Significantly, the metastable vaterite polymorph is only observed in the presence of a monolayer of **1**. The fact that vaterite is not observed under monolayers of **2** demonstrates that the formation of this polytype cannot be simply attributed to the kinetics as determined by the limited diffusion of NH_3 and CO_2 through the monolayer of **1**. Nevertheless, kinetics do play a role because Rieger et al.[39] did observe the subsequent formation of ACC and vaterite as transient phases following the mixing of aqueous solutions of calcium chloride and sodium carbonate.

The crystallization process is controlled by the template as evident from the formation of [00.1] oriented crystals vaterite. This is a gradual process as shown by the dark field TEM image (Figure 2e), which shows the coexistence of ACC and vaterite in a single particle. We suggest that, under the conditions used, the formation of the polar (00.1) vaterite face is mediated by the additional stabilization provided by the carboxylate groups of the monolayer.

The subsequent transformation into calcite involves a dissolution−reprecipitation mechanism as indicated by disappearance of vaterite particles concomitant with the formation of new, smaller calcite crystals. Interestingly, the observed orientations of both vaterite and calcite (i.e., [00.1] and [10.0], respectively) represent crystal faces in which the orientation of the carbonate ions is perpendicular to the nucleation plane. This suggests that the carboxylate groups may dictate the orientation of a first layer of carbonate ions in subsequently the (00.1) plane of vaterite and the (10.0) plane of calcite through interacting with a stern layer of calcium ions. As the (00.1) plane of vaterite has a charge density of about 6.7 calcium ions/nm^2, which is ∼2.5 times the charge density of a Langmuir monolayer of surfactant **1** (2.7 carboxylate groups/nm^2 as determined on a calcium bicarbonate subphase[40]), an epitaxial relationship between nucleating plane and template can be ruled out. It further implies that the exact compensation of the charge between the organic and inorganic phase is not a prerequisite to stabilize vaterite crystals. Nevertheless, the charge density of (10.0) calcite, which is 2.35 calcium ions/nm^2, is lower and gives a much better fit with the charge density of the monolayer. This may explain the transformation of (00.1) vaterite and the selection of (10.0) calcite as the preferred face.

Conclusions

In conclusion, we have demonstrated that cryoTEM in combination with SAED can be used to study the progression of the biomimetic formation of calcium carbonate under monolayers of a self-organized surfactant. This study has shown that irrespective of the presence of a dictating monolayer the formation of calcite is preceded by the formation of ACC as a transient precursor phase. We found that, in the presence of a templating monolayer, ACC first transformed into vaterite before a transformation into calcite occurred. The specificity of the interaction between the monolayer and the vaterite was demonstrated by the stabilization of a specific crystal plane: the (00.1) plane. Whereas the transformation of ACC to vaterite is a topotactic process involving an apparent solid-state transformation, the transformation of vaterite to calcite involved a dissolution−reprecipitation process. This sequence shows that under the monolayers of our valine-based surfactant the formation of calcium carbonate obeys the Ostwald−Lussac law, which predicts that the less dense, kinetically more accessible phases precede the dense, more thermodynamically stable phase.

The use of quasi-time-resolved cryoTEM analysis allows the quenching of the reaction and the trapping of the intermediate reaction products at precisely determined stages in the process. This procedure plays an important role in the detection of the early stages of the reaction. The technique further provided evidence that also in this biomimetic process the transient ACC can exist in more than one form with varying stability.

Acknowledgment. This research was supported by The Netherlands Scientific Organization (NWO). We thank L. Addadi and S. Weiner for inspiring discussions and D. C. Popescu, M. M. J. Smulders, and N. Chebotareva for providing compounds **1** and **2**.

Supporting Information Available: Additional TEM and SAED patterns and shape calculations. This material is available free of charge via the Internet at http://pubs.acs.org.

JA710416H

(39) (a) Rieger, J. *Tenside, Surfactants, Deterg.* **2002**, *39*, 221−225. (b) Rieger, J.; Frechen, T.; Cox, G.; Heckmann, W.; Schmidt, C.; Thieme, J. *Faraday Discuss.* **2007**, *136*, 265−277.

(40) See ref 5b. A Langmuir monolayer of surfactant **1** molecules formed on a calcium bicarbonate subphase was found to occupy a mean molecular area of about 38 Å^2 at zero pressure, which corresponds to a charge density of 2.7 carboxylate groups/nm^2.